# Shock Transition Solutions of Navier-Stokes Equations with Volume Viscosity for Nitrogen and Air

**M.K. Hryniewicki, J.J. Gottlieb, and C.P.T. Groth**

## 1 Introduction

The internal structure and transition solutions for planar shock waves based on solutions of the Navier-Stokes equations for diatomic and polyatomic gases are examined. The numerical solution of the steady, one-dimensional form of the Navier-Stokes equations describing compressible flows with full viscous and thermal heat conduction effects, including volume viscosity, are considered. The governing ordinary differential equations (ODEs) are solved to obtain the variation of temperature, pressure, density, flow velocity and entropy in both the physical and state planes, through shock waves of varying strength.

The ODE solutions for shock structure described above are compared to numerical predictions of shock wave transitions obtained using high-fidelity computational fluid dynamics (CFD). In particular, a parallel fully implicit finite-volume scheme with a Newton-Krylov-Schwarz (NKS) iterative solution method and anisotropic block-based adaptive mesh refinement (AMR) is used to obtain solutions to the multi-dimensional conservation form of the Navier-Stokes equations with volume viscosity. The anisotropic AMR scheme and efficient Newton method enable the rapid solution of the steady-state shock wave structure such that computational mesh densities for mesh-independent solutions can be readily established.

The effects of volume viscosity on both the internal structure and thickness of shock fronts are examined for several gases, including diatomic nitrogen ($N_2$), also previously considered by Elizarova *et al.* [1], as well as for air. The predicted shock structure and thickness for solutions including volume viscosity are shown to be in good agreement with experimental results for shock Mach numbers up to 6, demonstrating the importance of these additional effects on internal shock structures.

M.K. Hryniewicki · J.J. Gottlieb · C.P.T. Groth
Institute for Aerospace Studies, University of Toronto,
4925 Dufferin Street, Toronto, Ontario, Canada, M3H 5T6



R. Bonazza and D. Ranjan (eds.), *29th International Symposium on Shock Waves 2*,
DOI: 10.1007/978-3-319-16838-8_133

## 2 Navier-Stokes Equations

The Navier-Stokes equations governing laminar compressible gaseous flows, with and without volume viscosity, are used herein to examine the internal structure of shocks for diatomic and polyatomic gases. For a two-dimensional Cartesian coordinate system, $(x,y)$, these equations can be expressed in the following conservation form using matrix-vector notation:

$$\frac{\partial \mathbf{U}}{\partial t}+\frac{\partial \mathbf{F}}{\partial x}+\frac{\partial \mathbf{G}}{\partial y}=\frac{\partial \mathbf{F_v}}{\partial x}+\frac{\partial \mathbf{G_v}}{\partial y}, \tag{1}$$

where the vector of conserved solution variables, $\mathbf{U}$, inviscid flux vectors, $\mathbf{F}$ and $\mathbf{G}$, and viscous flux vectors, $\mathbf{F_v}$ and $\mathbf{G_v}$ are given by

$$\mathbf{U}=\begin{bmatrix}\rho\\ \rho u\\ \rho v\\ \rho E\end{bmatrix},\qquad \mathbf{F}=\begin{bmatrix}\rho u\\ \rho u^2+p\\ \rho uv\\ \rho u\left(E+\frac{p}{\rho}\right)\end{bmatrix},\qquad \mathbf{G}=\begin{bmatrix}\rho v\\ \rho uv\\ \rho v^2+p\\ \rho v\left(E+\frac{p}{\rho}\right)\end{bmatrix},$$

$$\mathbf{F_v}=\begin{bmatrix}0\\ \tau_{xx}\\ \tau_{xy}\\ -q_x+u\tau_{xx}+v\tau_{xy}\end{bmatrix},\qquad \mathbf{G_v}=\begin{bmatrix}0\\ \tau_{xy}\\ \tau_{yy}\\ -q_y+u\tau_{xy}+v\tau_{yy}\end{bmatrix}. \tag{2}$$

In Eq. (2), $\rho$ is the gas density, $u$ and $v$ are the $x$ and $y$ components of the flow velocity, and $E=e+\frac{1}{2}(u^2+v^2)$ is the specific total energy, where $e$ is the internal energy. The pressure is given by the ideal gas equation of state, $p=\rho RT$, where $R$ is the specific gas constant and $T$ is the temperature. The non-zero elements of the viscous stress tensor are

$$\tau_{xx}=\mu\left(\frac{4}{3}\frac{\partial u}{\partial x}-\frac{2}{3}\frac{\partial v}{\partial y}\right)+\mu_v\left(\frac{\partial u}{\partial x}+\frac{\partial v}{\partial y}\right),$$

$$\tau_{yy}=\mu\left(\frac{4}{3}\frac{\partial v}{\partial y}-\frac{2}{3}\frac{\partial u}{\partial x}\right)+\mu_v\left(\frac{\partial u}{\partial x}+\frac{\partial v}{\partial y}\right),\qquad \tau_{xy}=\mu\left(\frac{\partial u}{\partial y}+\frac{\partial v}{\partial x}\right), \tag{3}$$

for which $\mu$ and $\mu_v$ are the dynamic and volume viscosities of the gas, respectively. The $x$ and $y$ components of the heat flux vector, $q_x$ and $q_y$, are given by

$$q_x=-\kappa\frac{\partial T}{\partial x}\qquad\text{and}\qquad q_y=-\kappa\frac{\partial T}{\partial y}, \tag{4}$$

where $\kappa$ is the thermal conductivity. The dynamic viscosity and thermal conductivity for pure species and their mixtures are calculated according to the multicomponent mixture formulations employed by Gordon *et al.* [2]. Explicit expressions for the volume viscosity of pure species and their mixtures are adopted from Ern and Giovangigli [3] and gas properties and data are included from other sources [4–7].

## 3 ODE Solution Method for Shock-Wave Transitions

For the study of stationary planar shock waves, it is convenient to re-express the Navier-Stokes equations of Eq. (1) in an alternative non-dimensional form for a one-dimensional coordinate frame in which the direction normal to the shock is aligned with the $x$-coordinate direction. The resulting one-dimensional conservation equations governing the transport of mass, momentum, and energy through a steady shock are given by

$$D = \frac{U}{1+(\Gamma_s-1)(1-U)}, \qquad U-P = \left(\frac{4}{3}+\Omega_v\right)\frac{\mu}{\mu_1}\frac{\mathrm{d}U}{\mathrm{d}X},$$

$$\mathcal{T}-U = \frac{\Gamma_s-1}{\Gamma_s+1}(1-U)U - \left(\frac{4}{3}+\Omega_v\right)\frac{\mu}{\mu_1}\frac{2}{\Gamma_s+1}\frac{U}{D}\frac{\mathrm{d}U}{\mathrm{d}X} + \frac{\kappa}{\mu_1 c_p}\frac{\mathrm{d}\mathcal{T}}{\mathrm{d}X}, \tag{5}$$

where $\Omega_v = \mu_v/\mu$ is the ratio of volume and dynamic viscosities. The equation of state can also be re-written in non-dimensional form as

$$P = \frac{U+\frac{\gamma-1}{2\gamma}(\Gamma_s+1)(\mathcal{T}-U)}{1+(\Gamma_s-1)(1-U)}. \tag{6}$$

The various non-dimensional variables and constants that appear in Eqs. (5)–(6) are:

$$D = \frac{\rho-\rho_1}{\rho_2-\rho_1}, \quad U = \frac{u-u_1}{u_2-u_1}, \quad P = \frac{p-p_1}{p_2-p_1}, \quad \mathcal{T} = \frac{T-T_1}{T_2-T_1},$$

$$S = \frac{s-s_1}{s_2-s_1}, \quad X = \frac{\rho_1 u_1 x}{\mu_1}, \quad \Gamma_s = 1+\frac{M_s^2-1}{1+\frac{\gamma-1}{2}M_s^2}, \quad \mathrm{Pr}_1 = \frac{\mu_1 c_p}{\kappa_1}, \tag{7}$$

where $D$, $U$, $P$, $\mathcal{T}$, $S$, and $X$ are non-dimensional forms of the density, velocity, pressure, temperature, entropy, and distance normal to the shock, respectively. The parameter $\Gamma_s$ is the Rankine-Hugoniot jump relation for the density across a shock front, Pr is the Prandtl number, $M_s$ is the shock Mach number, $c_p$ is the specific heat at constant pressure, and $\gamma$ is the ratio of specific heats, taken to be equal to $7/5$ for both air and nitrogen. The subscripts 1 and 2 denote quasi-steady flow conditions in the regions ahead of and behind the shock front, respectively.

The solution of $U$ and $\mathcal{T}$ as a function of $X$ through the shock transition requires the simultaneous integration of two nonlinear ODEs having the form

$$\frac{\mathrm{d}U}{\mathrm{d}X} = \frac{3}{4+3\Omega_v}\frac{\mu_1}{\mu}\left[\frac{(\Gamma_s-1)(1-U)U - \frac{\gamma-1}{2\gamma}(\Gamma_s+1)(\mathcal{T}-U)}{1+(\Gamma_s-1)(1-U)}\right], \tag{8}$$

$$\frac{\mathrm{d}\mathcal{T}}{\mathrm{d}X} = \frac{\kappa_1}{\kappa}\frac{\mathrm{Pr}_1}{\Gamma_s+1}\left[\frac{1}{\gamma}(\Gamma_s+1)(\mathcal{T}-U)+(\Gamma_s-1)(1-U)U\right], \tag{9}$$

subject to appropriate boundary conditions (i.e., $0 \leq U \leq 1$ and $0 \leq \mathcal{T} \leq 1$). A fourth-order Runge-Kutta integration method is used to solve this coupled system. A numerical technique similar to that employed by Elizarova *et al.* [1] is utilized, wherein the transition solutions are solved first downstream and then upstream of the shock front, starting from the midpoint of the $U$ distribution. The variations of $D$, $P$ and $S$ with $X$ are then computed using the relations given above.

## 4 High-Fidelity CFD Solution Method

The ODE solutions for shock-front transitions described above are also compared herein to high-fidelity CFD solutions obtained using a parallel, fully implicit, finite-volume scheme with a NKS iterative solution method [8] and anisotropic block-based AMR [9] to solve the two-dimensional conservation form of the Navier-Stokes equations including the effects of volume viscosity. The anisotropic AMR scheme and efficient NKS method enable the rapid solution of steady-state shock-front structures such that computational mesh densities for mesh-independent solutions are readily established. As noted in the introduction, the comparisons of the ODE and high-fidelity CFD solutions provide a thorough verification of the two solution methods for predicting internal shock structures and allow for the establishment of mesh requirements for accurate and fully resolved CFD solutions of shock transition profiles.

## 5 Numerical Results and Conclusions

The smooth but rapid transition of non-dimensional flow properties through a shock-front of moderate strength $M_s = 2.62$ in air, computed using the ODE solution method, are presented in Fig. 1. Solutions in the physical plane on the left-hand side demonstrate that volume viscosity increases the localized dissipation in the shock front and produces a larger shock thickness. However, volume viscosity does not affect the Rankine-Hugoniot shock jump conditions, so the solution on either side of the shock front is unchanged with or without volume viscosity. The gradients of temperature, pressure, density and flow velocity within the shock front are thereby smaller when volume viscous effects are included. The smaller temperature gradient, in particular, results in a reduced localized heat conduction, which gives a lower entropy peak inside of the shock front, as illustrated. Solutions in the state plane are provided on the right-hand side of Fig. 1 and show the variation of non-dimensional flow properties as functions of the non-dimensional flow velocity.

The predicted reciprocal shock wave thicknesses, $\lambda/\Delta x$, computed from the ODE solutions for shock wave strengths of $1 \leq M_s \leq 6$ in air and nitrogen, are presented in Fig. 2. Experimental measurements for shock wave thicknesses in nitrogen that are available in the paper by Alsmeyer [10] are also included in Fig. 2, and they are represented using various symbols from previous experimenters. The mean free path, $\lambda$, has been defined from the kinetic theory of gases and is based on molecular collisions of rigid impenetrable spheres. The shock thickness, $\Delta x$, has been calculated from the velocity profile according to the standard maximum-slope thickness method of Becker [11] and others.

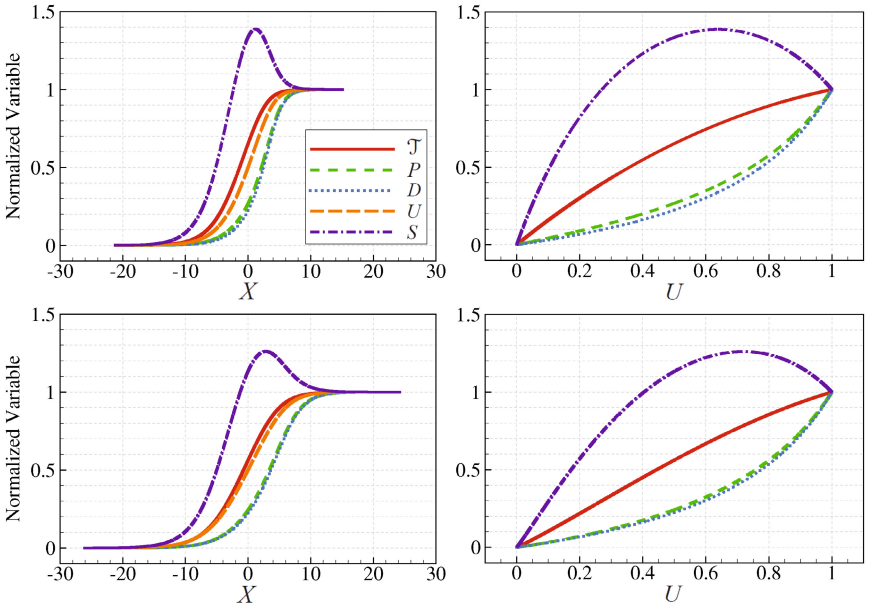


**Fig. 1** A comparison of both physical (left-hand side) and state (right-hand side) planes for a shock wave of strength $M_s = 2.62$ in air, for $\Omega_v = 0$ (top half) and $\Omega_v \neq 0$ (bottom half).

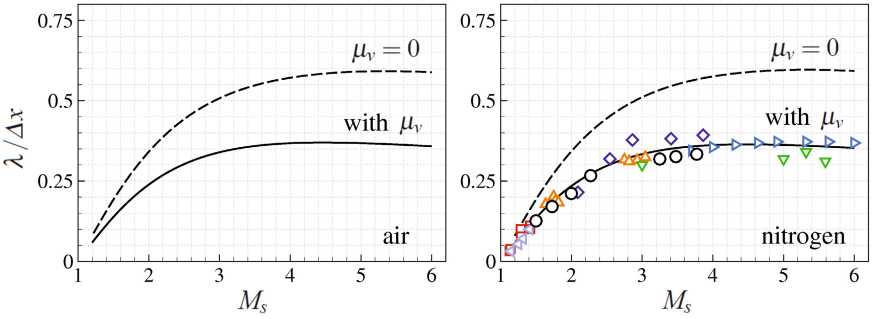


**Fig. 2** Reciprocal thickness comparisons for shock waves in air and nitrogen

In general, the reciprocal shock-wave thickness is expected to increase as a function of shock strength from weak to moderate shock waves and then plateaus for strong shocks. The numerical computations of shock thickness as obtained in this study over the range $1 \leq M_s \leq 6$ follow this pattern. Moreover, the shock-wave solutions are up to 48% thicker in air and nitrogen with the addition of volume viscosity as shown in Fig. 2. For nitrogen, the comparison of the ODE solutions for shock thickness to experimental measurements indicate that very good agreement between predictions and experiments can be achieved when volume viscosity is included. It would seem that the inclusion of volume viscosity in the Navier-Stokes equations

for compressible flow applications improves the continuum fluid-dynamic description of shock-front transitions by accounting for the rotational non-equilibrium behaviour of gases that occurs within a shock wave.

Although not shown here due to space limitations, it was also found that the high-fidelity CFD solution method using the parallel implicit finite-volume scheme was able to obtain shock-wave thicknesses that were typically accurate to within 0.05% of the results computed using the ODE solutions, when twenty-three levels of anisotropic AMR were used to fully resolve the shock front. It is believed this minor discrepancy is attributed solely to small numerical errors and possible differences in the modelling. The good agreement between the ODE solutions and CFD predictions provide a strong indication of appropriate computational mesh densities that are required for the numerical treatment of shock waves via a high-fidelity approach. In order to ensure the recovery of fully resolved, mesh-independent numerical shock-front transition solutions, the smallest cell sizes in a given computational domain must be on the order of $10^{-9}$ m, or 1 nm, for the nitrogen and air shocks considered herein under standard atmospheric conditions. Depending on the strength of the shock wave under investigation, this requires approximately $100 - 200$ cells to reside within the entire thickness of the shock front in a given CFD simulation.

## References

1. Elizarova, T.G., Khokhlov, A.A., Montero, S.: Numerical Simulation of Shock Wave Structure in Nitrogen. Phys. Fluids 19(6), 0681021–0681024 (2007)
2. Gordon, S., McBride, B.J., Zeleznik, F.J.: Computer Program for Calculation of Complex Chemical Equilibrium Compositions and Applications, Supplement 1 — Transport Properties. NASA-TM-86885 (1984)
3. Ern, A., Giovangigli, V.: Volume Viscosity of Dilute Polyatomic Gas Mixtures. Eur. J. Mech. B/Fluids 14(5), 653–669 (1995)
4. Hirschfelder, J.O., Bird, R.B., Spotz, E.L.: The Transport Properties for Non-Polar Gases. J. Chem. Phys. 16(10), 968–981 (1948)
5. Parker, J.G.: Rotational and Vibrational Relaxation in Diatomic Gases. Phys. Fluids 2(4), 449–462 (1959)
6. Chapman, S., Cowling, T.G.: The Mathematical Theory of Non-Uniform Gases, 3rd edn. Cambridge Press (1970)
7. Bird, G.A.: Molecular Gas Dynamics and the Direct Simulation of Gas Flows, 2nd edn. Oxford University Press (1994)
8. Groth, C.P.T., Northrup, S.A.: Parallel Implicit Adaptive Mesh Refinement Scheme for Body-Fitted Multi-Block Mesh. AIAA Paper 2005-5333 (2005)
9. Zhang, J.Z., Groth, C.P.T.: Parallel High-Order Anisotropic Block-Based Adaptive Mesh Refinement Finite-Volume Scheme. AIAA Paper 2011-3695 (2011)
10. Alsmeyer, H.: Density Profiles in Argon and Nitrogen Shock Waves Measured by the Absorption of an Electron Beam. J. Fluid Mech. 74(3), 497–513 (1976)
11. Becker, V.R.: Stoßwelle und Detonation. Zeit. Fur. Phys. 8, 321–362 (1921)